



**HAL**  
open science

## Improved CuGaSe<sub>2</sub> absorber properties through a modified co-evaporation process

Polyxeni Tsoulka, Adrien Rivalland, Ludovic Arzel, Nicolas Barreau

### ► To cite this version:

Polyxeni Tsoulka, Adrien Rivalland, Ludovic Arzel, Nicolas Barreau. Improved CuGaSe<sub>2</sub> absorber properties through a modified co-evaporation process. *Thin Solid Films*, 2020, 709, pp.138224. 10.1016/j.tsf.2020.138224 . hal-03010326

**HAL Id: hal-03010326**

**<https://hal.science/hal-03010326>**

Submitted on 22 Aug 2022

**HAL** is a multi-disciplinary open access archive for the deposit and dissemination of scientific research documents, whether they are published or not. The documents may come from teaching and research institutions in France or abroad, or from public or private research centers.

L'archive ouverte pluridisciplinaire **HAL**, est destinée au dépôt et à la diffusion de documents scientifiques de niveau recherche, publiés ou non, émanant des établissements d'enseignement et de recherche français ou étrangers, des laboratoires publics ou privés.



Distributed under a Creative Commons Attribution - NonCommercial 4.0 International License

# Improved CuGaSe<sub>2</sub> absorber properties through a modified co-evaporation process

Polyxeni Tsoulka, Adrien Rivalland, Ludovic Arzel, Nicolas Barreau

*Institut des Matériaux Jean Rouxel (IMN), UMR 6502 CNRS, Université de Nantes 2 rue de la Houssinière BP 32229, 44322 Nantes cedex 3, France.*

## Abstract

The present study deals with CuGaSe<sub>2</sub>-thin-films for solar cell applications. With the aim of achieving chemically and structurally homogeneous CuGaSe<sub>2</sub> layers, it is proposed a modified co-evaporation process, which implies two so-called relaxation sequences during films growth. The resulting layers are characterized by scanning electron microscopy and Raman spectroscopy. By comparing their characteristics with those of CuGaSe<sub>2</sub> grown without relaxation sequence, it is demonstrated that the modified process yields improved distribution of elements throughout the whole layer. The performance of the resulting solar cells is improved exclusively through increased quantum efficiency in the large wavelengths; further output voltage increase would require alternative junction partners.

**Keywords:** Copper gallium di-selenide; Co-evaporation process; Thin films; Wide band gap; Copper ratio; Physical vapor deposition

## 1. Introduction

Solar cell technology based on polycrystalline CuIn<sub>1-x</sub>Ga<sub>x</sub>Se<sub>2</sub> (CIGSe) chalcopyrite thin film has reached an outstanding level of energy conversion efficiency [1]. A major interest of CuIn<sub>1-x</sub>Ga<sub>x</sub>Se<sub>2</sub> semiconductor remains its band gap tunability with x; it can indeed be varied from E<sub>g</sub>=1.04 eV (x=0, CuInSe<sub>2</sub>) through E<sub>g</sub>=1.68 eV (x=1, CuGaSe<sub>2</sub>) [2,3]. This wide range of achievable band gap energies yields these materials receiving a growing attention as potential partner in multi-junction solar cell technology as well as materials for the development of advanced concepts [4]. In particular, the

compound showing the widest band gap ( $E_g$ ), namely CGSe with  $E_g$  close to 1.7 eV, appears to be a good candidate as top cell material for tandem applications combined with the already mature c-Silicon technology [4].

Up to date, the best efficiencies are achieved from narrow band gap CIGSe (22.6 % [1]), corresponding to  $x$  lower than 0.4. This experimental fact is in contradiction with the theoretical expectations, which predict optimal performance for  $x \sim 0.7$  ( $E_g$  close to 1.4 eV). Many studies showed that when  $x > 0.4$ , the open circuit voltage ( $V_{oc}$ ) does not follow a linear increase with  $x$ , which results in lowered device performance [5]. So far, the best In-free CGSe-based cell efficiency ever reported does not exceed 11.9 % [6]. For more than two decades, numerous models were proposed to explain the hindered performance at large  $x$ . Basically, the reasons given are *i*) the existence of Cu-enriched grain boundaries [7], *ii*) the cliff-like CIGSe/CdS interface band structure [6,8,9] and *iii*) the increased concentration of the trap states within the bulk of the film [10,11].

Several experimental investigations on so-called wide gap ( $x$  between 0.5 and 1) C(I)GSe layers report on the presence of detrimental Cu-enriched secondary phases within the bulk [12,13] of the film, as well as at the grain boundaries; whereas none of these phases are detected within narrow band gap ( $x < 0.4$ ) CI(G)Se layers [7,14,15]. These observations contrast with the phase diagrams of the ternary [16,17] (CISE, CGSe) and quaternary [18] (CIGSe) compounds, which suggest a homogeneous chalcopyrite structure close to the stoichiometry (*i.e.* no co-existence of both Cu-rich and Cu-poor secondary phases). The origin of this contradiction between experimental observations and phase diagrams probably originates from the fact that CIGSe thin films growth (whatever the technique) takes place under non-equilibrium conditions. In addition, studies on CISE and CGSe reaction kinetics [19–22] relate that the activation energy of CGSe is almost two times larger than that of CISE; which, at a given temperature, yields much slower CGSe formation compared to CISE. Therefore, to overcome local inhomogeneities issues in wide

band gap C(I)GSe, and thereby expect improved solar cell performance, one needs to adapt the CIGSe deposition process to both the thermodynamic and kinetic needs of the high Ga-containing absorbers.

Up to now, most of the reports relative to chalcopyrite thin film growth process focus on narrow gap CIGSe. The present study aims at re-investigating a three-step co-evaporation process to achieve structurally and chemically homogeneous CGSe absorber layer. Our approach relies on reaching thermodynamic equilibrium by applying relaxation sequences during key-steps of the growth. The local inhomogeneities/secondary phases throughout the resulting CGSe layers are investigated by means of micro-Raman spectroscopy at excitation wavelength close to CGSe band gap.

The paper is organized as follows: Section 2 describes the experimental methods used for the synthesis and characterization of the layers and related solar cells. The results are presented in the section 3 and further discussed in section 4. Conclusions are drawn in the final section.

## **2. Experimental**

### **2.1 CGSe co-evaporation process and solar cells fabrication**

In this study, thin-film solar cells consist of the following layers stack Mo/CGSe/CdS/ZnO/ZnO:Al deposited on 1 mm-thick soda-lime glass (SLG) substrate. CGSe absorbers are co-evaporated from elemental sources using the sequential CuPRO process. This latter, originally proposed by J. Kessler [23] is a modified 3-stage process, which herein consists in keeping the gallium flux constant and varying copper flux so that the nominal composition of the growing film follows Cu-Poor/Cu-Rich/Cu-Poor transitions [23]. The Cu-poor and Cu-rich compositions correspond to  $x = [Cu]/[Ga] < 1$  and  $x > 1$  respectively. The targeted final composition of the films corresponds to copper to gallium ratio close to 0.9, and layers thickness is 1.6  $\mu\text{m}$ . During the whole deposition process, (i) a strong excess Se flux compared to metal fluxes ( $\Phi_{\text{Se}}/\Phi_{\text{Metals}} > 20$ ) is provided, and (ii) SLG/Mo substrates temperature is kept constant at 580°C.

To remove eventual copper-selenide and gallium-oxide secondary phases from CGSe surface, all SLG/Mo/CGSe structures were chemically etched using a 0.1M KCN aqueous solution [24] for 5 min at room temperature. The etched samples were then rinsed with deionized water before being covered with 40 nm-thick CdS buffer layer deposited by chemical bath deposition (CBD). For more information about the CBD process see references [8,25,26]. Finally, a window consisting of ZnO(50 nm)/ZnO:Al(150 nm) bilayer was RF-sputtered from ceramic targets, and metallic (Ni/Al/Ni) grids designed for 0.5 cm<sup>2</sup> solar cells were electron beamed through a shadow mask. These completed devices were annealed in air for 2 min at 200 °C.

In this study, a modified CuPRO process (CuPRO(M)) was also investigated; it consists in applying two so-called relaxation periods during the following key-steps of the deposition process: after the growing films turned Cu-rich (*i.e.* at the end of the 2<sup>nd</sup> stage), and when the growth is completed (*i.e.* at the end of the deposition process). During each of these relaxation periods, all sources are shuttered for 30 min while substrates kept at 580 °C. The characteristics of all investigated samples are described in Table I.

## 2.2 Characterization methods

The elemental composition of the CGSe layers was measured by EDS (X-ray Energy Dispersive Spectroscopy) using a JEOL JSM 5800LV scanning electron microscope (SEM) equipped with a Ge-detector. The EDS analyses were carried out at 20 kV acceleration voltage, which corresponds to a bulk analysis with 1.3 μm penetration depth. The high-resolution SEM images were taken using a JEOL JSM 7600F.

The vibrational structure of CGSe and the identification of secondary phases at the first 150 nm from the surface and from the back contact were investigated using Raman spectroscopy at 633 nm excitation wavelength. The instrument employed is a Renishaw InVia Reflex microscope and a He-Ne laser source.

The laser power and the acquisition time were optimized in order to avoid possible heating effects or deterioration of the analyzed region.

The Raman analysis at the back CGSe surface was performed after lifting the CGSe layer off of the SLG/Mo substrate. To lift the CGSe off of the Mo rear-contact, epoxy glue was applied at the CGSe surface and then a SLG was placed on the top of the CGSe layer. SLG/Mo/CGSe/epoxy/SLG was then annealed at 80°C for one hour to polymerize the epoxy. Finally applying an opposite small lateral strain between the two SLGs the SLG/epoxy/CGS and SLG/Mo were easily separated, leaving the CGSe rear surface clear for further analyses. A schematic representation of this CGSe lift-off procedure is shown in figure 1.

CGSe solar cells photovoltaic parameters, namely open circuit voltage ( $V_{oc}$ ), short-circuit current density ( $J_{sc}$ ), fill factor (FF) were determined from current density-voltage ( $J(V)$ ) characteristics acquired at 25 °C under AM1.5 illumination at 1000 W/m<sup>2</sup> intensity. Integration of external quantum efficiency (EQE, laboratory built) led to actual values of  $J_{sc}$ .

### **3. Results**

#### **3.1 Insights on the CGSe homogeneity using Raman analysis**

Figures 2a and 2b present the Raman spectra acquired at the top and the rear surface of the CGSe films deposited by the CuPRO (Fig. 2)) and the CuPRO(M) methods (Fig. 2b). The Raman modes of the CGSe structure are indicated by the black squares and the ordered vacancy compound by the blue squares.

The  $A_1$ -Raman mode at 185 cm<sup>-1</sup> corresponds to the motion of Se against the Cu and the Ga at rest and the  $E_1$ -mode at 274 cm<sup>-1</sup> is related to the in-phase motion of the cations against the Se [27]. These two vibrational modes are strongly influenced by the concentration of the point defects, therefore by the

[Cu]/[Ga] ratio and by the order-disorder phase transitions [28,29]. More precisely, for excitation wavelength close to the band gap of CGSe, increasing the Ga content relative to Cu in the absorber layer yields *i*) an increased intensity of the E<sub>1</sub>-mode with respect to the A<sub>1</sub>-mode and *ii*) a widening of both the A<sub>1</sub> and E<sub>1</sub> Raman peaks. Xue *et al.* [28] also reported that the intensity ratio ( $\Gamma = I_{E1}/I_{A1}$ ) loops the relative Ga to Cu ratio; basically  $\Gamma$  is smaller than unity when the Cu content is high ([Cu]/[Ga] > 1) and greater than unity when the Cu content is low. In this latter case, the full width at half maximum (FWHM) of the peaks increases due to the order-disorder transition [28].

Structural and chemical homogeneity throughout the films was evaluated using Raman spectroscopy with an excitation wavelength close to the band gap of CGSe; specific attention is paid on the FWHM and the intensity ratio of the A<sub>1</sub> and E<sub>1</sub> vibrational modes. A comparison of the Raman spectra from rear and top CGSe surfaces of the films grown by either the regular CuPRO process or the modified CuPRO (*i.e.* CuPRO(M)) emphasizes the following:

- 1) In the case of the CGSe film grown by the CuPRO(M) method,  $\Gamma$  is greater than 1 and is similar at both rear and top surfaces (see Fig. 3a and 3b); this means the same slightly Ga-rich chalcopyrite phase is present at both the top and rear sides of the CGSe layer. In contrast, the spectra from sample grown by the regular CuPRO process show different  $\Gamma$  at the top and rear sides of the layer; it exceeds 1 at the top and is lower than 1 at the rear. This observation suggests the composition throughout the CGSe layer is not uniform; the Cu content is higher close to the back contact.
- 2) The same conclusions can be drawn by comparing the FWHM of A<sub>1</sub> and E<sub>1</sub> Raman modes (see Fig. 3c and 3d); similar FWHM are observed at both sides of the film fabricated by CuPRO(M) while CuPRO yields different FWHM. This result corroborates previous findings indicating the amount of Cu vacancies differs from rear toward top side of the CGSe layer grown by CuPRO and emphasize the composition is not uniform throughout the absorber.

3) The surface of the film grown by standard CuPRO is inhomogeneous, Cu-poor secondary phases co-exist with stoichiometric CGSe phase. Dashed lines of Fig. 2 show the Raman bands assigned to Cu-poor  $\text{CuGa}_3\text{Se}_5$  and CGSe chalcopyrite structure. These structural/chemical/morphological inhomogeneities are visible in the SEM plan-view shown in Fig. 4a; the larger grains are close-to-stoichiometry CGSe, whereas the areas with the smaller grains are Cu-poor ( $\text{CuGa}_3\text{Se}_5$ ). In contrast, the surface of the film grown by CuPRO(M) (see Raman spectra Fig. 2b) is made of a homogeneously distributed slightly Cu-poor chalcopyrite. The representative SEM image depicted Fig. 4b, showing large grains with a characteristic stepped patterned morphology, corroborates this conclusion.

The schematics drawn in Fig. 3 illustrate such variations of Cu contents for films deposited by either CuPRO (Fig. 3e) or CuPRO(M) (Fig. 3f).

### 3.2 CGSe solar cells

Fig. 5 plots the photovoltaic parameters ( $V_{oc}$ ,  $J_{sc}$ , FF and  $\eta$ ) of solar cells fabricated from CGSe absorbers grown by either CuPRO or CuPRO(M) process, as described in section 2. These results show that applying CuPRO(M) yields improved device efficiency. However, the parameter mainly improved is neither the  $V_{oc}$  nor the FF, but the  $J_{sc}$  as illustrated by the EQE plotted in Fig. 6. These latter curves, from the best devices, point out that the gain in  $J_{sc}$  is due to improved EQE in the large-wavelength region [500 nm - 800 nm]. This observation suggests the dominant limitation of absorbers grown by CuPRO could be a hindered collection of carriers photo-generated close to the back contact. Moreover, the inset plot of  $[E \cdot \ln(1-EQE)]^2$  versus Energy of photons, indicates that the band gap energy is the same in both the CuPRO and the CuPRO(M) based absorber; the band gap energy difference between the two absorbers is 0.005 eV ( $E_g = 1.665$  eV and 1.670 eV for the the CuPRO(M) and CuPRO based absorber, respectively). Hence, the different Cu distribution through the CuPRO-CGSe and the CuPRO(M)-CGSe



layer does not affect the band gap of the material. This result has further strengthened our conviction that the gain in  $J_{sc}$  of the CuPRO(M)-CGSe cell is not due to a different band gap but rather, to an improved carrier collection close to the back contact. In addition, the statistical plots of Fig. 5, each gathering the parameters of 10 cells from the same slot, reveal a much wider dispersion of  $V_{oc}$  and FF values in the case of cells based on regular CuPRO method. A comparison between two best solar cells containing an  $MgF_2$  anti-reflecting coating is shown in table II.

## 4. Discussion

The growth of high Ga-containing CIGSe thin films has specific kinetic and thermodynamic issues. Accordingly, a modified co-evaporation process, implying two relaxation sequences, is proposed herein to attempt reaching the thermodynamic equilibrium and thereby expect fabricating structurally and chemically homogeneous absorbers.

Previous studies on CGSe layers reported improved solar cell performance with increased substrates temperature (about 650 °C) [5] during deposition. According to [5,6], this gain is inherent to the quality of the absorber because:

- i)* the alloy solubility is increased or/and
- ii)* the grains are larger, therefore the density of GBs acting as recombination centers decreases,
- iii)* the nature of the GBs is likely to turn from detrimental at low temperature to beneficial (passivation of defects at the vicinity of the GBs) at higher growth temperatures.

In this work, it is demonstrated that substrate temperature is probably not the only key-parameter yielding improved CGSe-based device efficiency, meaning the formation of homogeneous CGSe layers rather relies on kinetic than thermodynamic concerns. Indeed, the CGSe layers, either grown by CuPRO or CuPRO(M), have similar overall composition. However, the Cu content is much higher at the rear

side of CuPRO layer compared to its front side. As a consequence, the amount of structural defects is likely severely different at the front and rear sides of the absorber. In contrast, CuPRO(M) growth process, implying so-called relaxation sequences, results in CGSe layer with similar Cu-content at both top and rear sides. Therefore, leaving the system at 580 °C for a while yields homogenization of Cu and Ga distribution, thus higher quality material, which supports the hypothesis of kinetic issues.

As far as devices are concerned, the reduced effective carrier collection measured at large wavelengths in CuPRO-CGSe based cell suggests the absorber portion harming the current is close to the back contact. Correlating this result with CuPRO-layers chemical characteristics, one may conclude the CGSe portion closer to the rear contact, which is Cu-enriched, does not participate to the generation of current as already suggested by M.A. Contreras *et al.* [5]. Indeed, Cu-excess is likely to segregate at the grain boundaries or form localized  $\text{Cu}_x\text{Se}$  clusters, both yielding either shunt path or junction electric field screening [7,12,30,31]. Although showing about 2 mA/cm<sup>2</sup> higher current density, CuPRO(M)-CGSe based cell performance is still limited by low FF and high  $V_{oc}$  deficit compared to theoretical expectations. The latter  $V_{oc}$  deficit is most probably due to the inadequate band alignment at CGSe/CdS interface [6,32]; indeed, the negative conduction band offset (cliff-like) at the CGSe/CdS junction is known to yield severe interface recombination and thereby strongly hinder the output voltage of the solar cell. Consequently, an alternative buffer layer should be applied to further improve the performance of CuPRO(M)-CGSe based devices [33].

## 5. Conclusions

Considering the higher activation energy and the lower reaction rates of CGSe compared to CISE, methodologies and co-evaporation strategies should be envisaged to improve CGSe-based cell performance. In the present work, it is proposed a modified CuPRO(M) process consisting in applying relaxation sequences during CGSe layers co-evaporation. In our proposed scenario, it is demonstrated

these sequences compensate the harming slow kinetic of CGSe formation, and enhance both short and long-range resulting distribution of metal atoms throughout the layer. The CuPRO(M) process exhibits *i*) larger grains *ii*) improved lateral uniformity of the surface and *iii*) close to stoichiometry rear surface. Hence it seems that applying two relaxation stages during the deposition process, we can achieve a more uniform distribution of the metal atoms in the CGSe thin films.

In addition to a sharper distribution of photovoltaic parameters, the modified process reduces the recombination at the CGSe/CdS and Mo/CGSe interfaces and leads to improved solar cell performance due to the gain in current density, inherent to a better quantum efficiency close to the band gap energy. Nevertheless, although the properties of absorbers bulk are improved, the performances of the cells are still limited by a severe  $V_{oc}$  deficit assigned to a non-suitable CGSe/CdS interface. As a conclusion, one should develop better adapted n-type junction partner to fully take the advantage of the improved CGSe bulk characteristics.

## **Acknowledgements**

This work was supported by the Jean Rouxel Institute of materials and the University of Nantes. We gratefully acknowledge the help provided by Lionel Assmann, and Nicolas Stephant for his technical assistance for the SEM observations.

## Appendix A

### A.1: CuPRO and CuPRO(M) co-evaporation processes

The CuPRO is a three-step process based on a Cu-Poor/Cu-Rich/Cu-poor transition of the film composition during the growth. In our samples the vapor flux of the metals ( $\Phi$  in  $atoms \cdot cm^{-2} \cdot s^{-1}$ ) is controlled in order to have  $\Phi_{Cu}/\Phi_{Ga} \approx 0.8$  during of the first (Cu-poor) co-evaporation step and  $\Phi_{Cu}/\Phi_{Ga} \approx 1.5$  during the second (Cu-rich) co-evaporation step. At the final (Cu-poor) third stage the evaporation of Cu is interrupted and the excess of Cu is consumed by the Ga and Se provided by the sources. During the process the Se flux is in excess. A graphical representation of the standard CuPRO co-evaporation process is shown in Fig. A.1 (a).

In our work, we have also studied a modified CuPRO process (CuPRO(M)). A graphical representation of the modified CuPRO(M) co-evaporation process is shown in Fig. A.1 (b)).

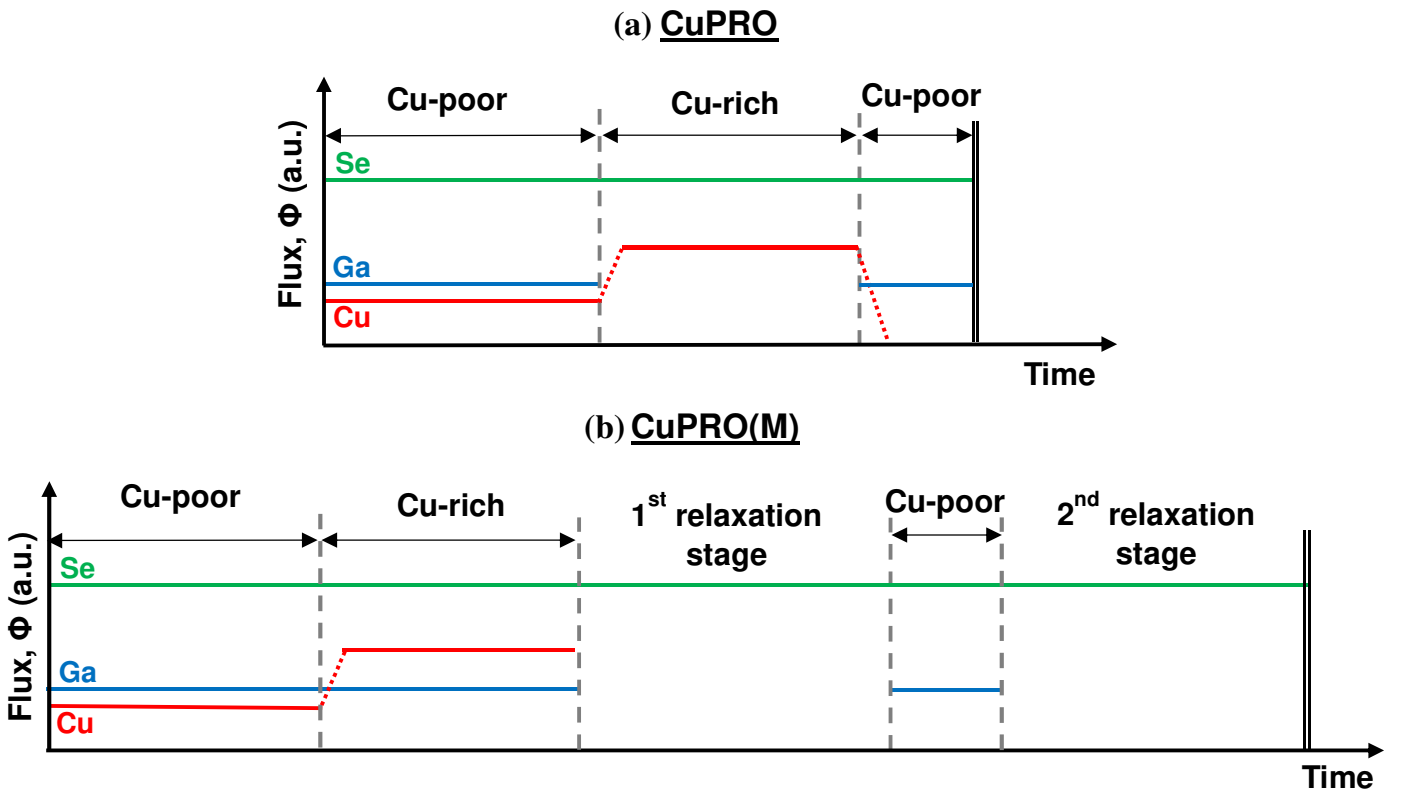


Figure A.1: Graphical representation of the CuPRO and CuPRO(M) processes

## **A.2: Relaxation mechanism: composition, morphology and diffusion**

In the CuPRO(M) process we applied two relaxation stages :

- The first relaxation stage is introduced after the end of the Cu-rich co-evaporation stage.



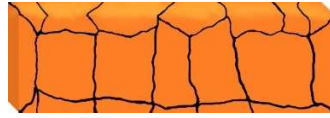


The main purpose of this relaxation stage is the segregation of the whole Cu at the surface of the film in order to obtain a uniform Cu/Ga distribution within the bulk of the material. Moreover, the relaxation stage leads to grain enlargement and hence reduces the number of grain boundaries which act as recombination centers and deteriorate the solar cell performance.

- The second relaxation stage is applied at the end of the co-evaporation process after the Cu-poor stage.

The duration of the Cu-poor stage is around 9 minutes. Since the homogeneity of the absorber is thermodynamic and kinetic issue, the duration of the Cu-poor stage is too small to allow Ga provided by the sources, to diffuse deeper within the bulk of the layer and closer to the back contact. In other words, the duration of the Cu-poor stage is not sufficient to make the Ga diffuse and consume the whole excess of Cu which can be present at the rear surface of the film. Hence, applying a second relaxation stage, we facilitate the diffusion of Ga presented in the upper surface, towards the bulk of the material. The enhanced Cu/Ga intermixture leads also to an additional grain growth.

Table A.I shows a detailed schematic representation of the composition and the morphology (size of the grains) of the absorber synthesized using the CuPRO and the CuPRO(M) co-evaporation process.

**Table A.I :** Schematic representation of the structure (relative size of the grains) and the composition (red: Cu-rich, orange: stoichiometric, yellow: Cu-poor) of the absorber at the end of each co-evaporation (Cu-rich and Cu-poor) or relaxation stage (the first one after the Cu-rich stage and second one at the end of the process, only in the CuPRO(M)). The CuPRO process does not have any relaxation stage

Process	Cu-rich stage	1 <sup>st</sup> relaxation stage	Cu-poor stage and 2 <sup>nd</sup> relaxation stage (end of the process)
CuPRO(M)			
Comments	<p>1) The chalcopyrite phase (orange) co-exists with the Cu-Se secondary phases (red)</p> <p>2) The distribution of Cu is not homogeneous</p>	<p>1) The Cu/Ga interdiffusion is enhanced leading to grain growth</p> <p>2) The excess of Cu segregates at the surface resulting in a stoichiometric bulk and a Cu-rich surface</p>	<p>1) The Ga-Se provided by the sources consumes the excess of Cu of the surface</p> <p>2) The relaxation enhance the grain growth, annihilates the voids and leads to a more uniform Cu/Ga distribution</p>
Process	Cu-rich stage	Without relaxation	Cu-poor stage Without relaxation (end of the process)
CuPRO		-	
Comments	<p>1) The chalcopyrite phase (orange) co-exists with the Cu-Se secondary phases (red)</p> <p>2) The distribution of Cu is not homogeneous</p>		<p>The duration of the Cu-poor stage is not sufficient to make the whole Cu segregate at the surface or/and the Ga to diffuse deeper, close to the rear surface. The final layer is not uniform; it has Cu-poor top surface and Cu-rich rear surface</p>

## References

- [1] P. Jackson, R. Wuerz, D. Hariskos, E. Lotter, W. Witte, M. Powalla, Effects of heavy alkali elements in Cu(In,Ga)Se<sub>2</sub> solar cells with efficiencies up to 22.6%, *Phys. Status Solidi - Rapid Res. Lett.* 10 (2016) 583–586. <https://doi.org/10.1002/pssr.201600199>.
- [2] T. Tinoco, C. Rincón, M. Quintero, G.S. Pérez, Phase Diagram and Optical Energy Gaps for CuIn<sub>y</sub>Ga<sub>1-y</sub>Se<sub>2</sub> Alloys, *Phys. Status Solidi.* 124 (1991) 427–434. <https://doi.org/10.1002/pssa.2211240206>.
- [3] S.H. Wei, S.B. Zhang, A. Zunger, Effects of Ga addition to CuInSe<sub>2</sub> on its electronic, structural, and defect properties, *Appl. Phys. Lett.* 72 (1998) 3199–3201. <https://doi.org/10.1063/1.121548>.
- [4] A.R. Jeong, S. Bin Choi, W.M. Kim, J.K. Park, J. Choi, I. Kim, J.H. Jeong, Electrical analysis of c-Si/CGSe monolithic tandem solar cells by using a cell-selective light absorption scheme, *Sci. Rep.* 7 (2017) 1–10. <https://doi.org/10.1038/s41598-017-15998-y>.
- [5] W.M. Miguel A. Contreras, Lorelle M. Mansfield, Brian Egaas Jian Li, Manuel Romero, Rommel Noufi, Eveline Rudiger-Voigt, Wide bandgap Cu(In,Ga)Se<sub>2</sub> solar cells with improved energy conversion efficiency, *Prog. Photovoltaics Res. Appl.* (2012). <https://doi.org/10.1002/pip.2244>.
- [6] F. Larsson, N.S. Nilsson, J. Keller, C. Frisk, V. Kosyak, M. Edoff, T. Törndahl, Record 1.0 V open-circuit voltage in wide band gap chalcopyrite solar cells, *Prog. Photovoltaics Res. Appl.* 25 (2017) 755–763. <https://doi.org/10.1002/pip.2914>.
- [7] M. Raghuvanshi, Influence of Grain Boundary Chemistry on the properties of CIGS photovoltaic cells, Rouen, 2016.
- [8] R. Caballero, C.A. Kaufmann, M. Cwil, C. Kelch, D. Schweigert, T. Unold, M. Rusu, H.W. Schock, S. Siebentritt, The role of the CdS buffer layer in CuGaSe<sub>2</sub>-based solar cells, *J. Phys. Condens. Matter.* 19 (2007) 356222. <https://doi.org/10.1088/0953-8984/19/35/356222>.
- [9] M. Rusu, M. Bär, D.F. Marrón, S. Lehmann, T. Schedel-Niedrig, M.C. Lux-Steiner, Transport properties of CuGaSe<sub>2</sub>-based thin-film solar cells as a function of absorber composition, *Thin Solid Films.* 519 (2011) 7304–7307. <https://doi.org/10.1016/j.tsf.2011.01.185>.
- [10] U. Rau, M. Schmidt, A. Jasenek, G. Hanna, H.W. Schock, Electrical characterization of Cu(In,Ga)Se<sub>2</sub> thin-film solar cells and the role of defects for the device performance, *Sol. Energy Mater. Sol. Cells.* 67 (2001) 137–143. [https://doi.org/10.1016/S0927-0248\(00\)00273-7](https://doi.org/10.1016/S0927-0248(00)00273-7).
- [11] G. Hanna, A. Jasenek, U. Rau, H.W. Schock, Influence of the Ga-content on the bulk defect densities of Cu(In,Ga)Se<sub>2</sub>, *Thin Solid Films.* 387 (2001) 71–73. [https://doi.org/10.1016/S0040-6090\(00\)01710-7](https://doi.org/10.1016/S0040-6090(00)01710-7).
- [12] E. Simsek Sanli, Q.M. Ramasse, R. Mainz, A. Weber, D. Abou-Ras, W. Sigle, P.A. van Aken, Evidence for Cu<sub>2-x</sub>Se platelets at grain boundaries and within grains in Cu(In,Ga)Se<sub>2</sub> thin films, *Appl. Phys. Lett.* 111 (2017) 032103. <https://doi.org/10.1063/1.4993917>.
- [13] D.F. Marrón, T. Glatzel, A. Meeder, T. Schedel-Niedrig, S. Sadewasser, M.C. Lux-Steiner, Electronic structure of secondary phases in Cu-rich CuGaSe<sub>2</sub> solar cell devices, *Appl. Phys. Lett.* 85 (2004) 3755–3757. <https://doi.org/10.1063/1.1812582>.
- [14] M. Raghuvanshi, E. Cadel, P. Pareige, S. Duguay, F. Couzinie-Devy, L. Arzel, N. Barreau, Influence of grain boundary modification on limited performance of wide bandgap Cu(In,Ga)Se<sub>2</sub> solar cells, *Appl. Phys. Lett.* 105 (2014) 013902. <https://doi.org/10.1063/1.4890001>.
- [15] C. Jiang, R. Noufi, J.A. Abushama, K. Ramanathan, H.R. Moutinho, J. Pankow, C. Jiang, R.

- Noufi, J.A. Abushama, K. Ramanathan, H.R. Moutinho, J. Pankow, Local built-in potential on grain boundary of Cu (In, Ga)Se<sub>2</sub> thin films, 84 (2016) 16–19. <https://doi.org/10.1063/1.1737796>.
- [16] T. Maeda, W. Gong, T. Wada, Crystallographic and optical properties and band structures of CuInSe<sub>2</sub>, CuIn<sub>3</sub>Se<sub>5</sub> and CuIn<sub>5</sub>Se<sub>8</sub> phases in Cu-poor Cu<sub>2</sub>Se – In<sub>2</sub>Se<sub>3</sub> pseudo-binary system compounds, Japan Soc. Appl. Phys. 55 (2016).
- [17] J.C. Mikkelsen, Ternary phase relations of the chalcopyrite compound CuGaSe<sub>2</sub>, J. Electron. Mater. (1981). <https://doi.org/10.1007/BF02654590>.
- [18] C. Beilharz, Charakterisierung von aus der Schmelze gezüchteten Kristallen in den Systemen Kupfer-Indium-Selen und Kupfer-Indium-Gallium-Selen für photovoltaische Anwendungen, Shaker Verlag, 1999.
- [19] S. Kim, W.K. Kim, R.M. Kaczynski, R.D. Acher, S. Yoon, T.J. Anderson, O.D. Crisalle, E. a. Payzant, S.S. Li, Reaction kinetics of CuInSe<sub>2</sub> thin films grown from bilayer InSe/CuSe precursors, J. Vac. Sci. Technol. A Vacuum, Surfaces, Film. 23 (2005) 310. <https://doi.org/10.1116/1.1861051>.
- [20] W.K. Kim, E.A. Payzant, S. Kim, S.A. Speakman, O.D. Crisalle, T.J. Anderson, Reaction kinetics of CuGaSe<sub>2</sub> formation from a GaSe/CuSe bilayer precursor film, J. Cryst. Growth. 310 (2008) 2987–2994. <https://doi.org/10.1016/j.jcrysgro.2008.01.034>.
- [21] M. Marudachalam, R.W. Birkmire, H. Hichri, J.M. Schultz, A. Swartzlander, M.M. Al-Jassim, Phases, morphology, and diffusion in CuIn<sub>x</sub>Ga<sub>1-x</sub>Se<sub>2</sub> thin films, J. Appl. Phys. 82 (1997) 2896–2905. <https://doi.org/10.1063/1.366122>.
- [22] H. Dittrich, U. Prinz, J. Szot, W.H. Schock, Analysis of reaction kinetics of selenized CuInSe<sub>2</sub> and CuGaSe<sub>2</sub> thin films, Proc. 9th EC Photovolt. Sol. Energy Conf. (1989).
- [23] J. Kessler, C. Chityuttakan, J. Lu, J. Scholdstrom, L. Stolt, Cu(In,Ga)Se<sub>2</sub> thin films grown with a Cu-poor/rich/poor sequence: Growth model and structural considerations, Prog. Photovoltaics Res. Appl. 11 (2003) 319–331. <https://doi.org/10.1002/pip.495>.
- [24] J. Lehmann, S. Lehmann, I. Lauermaun, T. Rissom, C.A. Kaufmann, M.C. Lux-Steiner, M. Bär, S. Sadewasser, Reliable wet-chemical cleaning of natively oxidized high-efficiency Cu(In,Ga)Se<sub>2</sub> thin-film solar cell absorbers, J. Appl. Phys. 116 (2014). <https://doi.org/10.1063/1.4903976>.
- [25] V. Nadenau, D. Hariskos, H.-W. Schock, M. Krejci, F.-J. Haug, A.N. Tiwari, H. Zogg, G. Kostorz, Microstructural study of the CdS/CuGaSe<sub>2</sub> interfacial region in CuGaSe<sub>2</sub> thin film solar cells, J. Appl. Phys. 85 (1999) 534–542. <https://doi.org/10.1063/1.369486>.
- [26] J. Kessler, K.-O. Velthaus, M. Ruckh, R. Laichinger, H.-W. Schock, D. Lincot, R. Ortega, J. Vedel, Chemical bath deposition of CdS on CuInSe<sub>2</sub>, etching effects and growth kinetics, Proc. 6th Int. Photovolt. Sci. Eng. Conf. (1992).
- [27] C. Rincón, F.J. Ramírez, Lattice vibrations of CuInSe<sub>2</sub> and CuGaSe<sub>2</sub> by Raman microspectrometry, 72 (1992) 4321–4324. <https://doi.org/10.1063/1.352195>.
- [28] C. Xue, D. Papadimitriou, N. Esser, Mapping of gradient composition Cu<sub>x</sub>Ga<sub>y</sub>Se<sub>2</sub> film properties using Raman and PL-spectroscopy, J. Phys. D. Appl. Phys. 37 (2004) 2267–2273. <https://doi.org/10.1088/0022-3727/37/16/008>.
- [29] C. Xue, D. Papadimitriou, Y.S. Raptis, N. Esser, W. Richter, S. Siebentritt, M.C. Lux-Steiner, Compositional dependence of Raman scattering and photoluminescence emission in Cu<sub>x</sub>Ga<sub>y</sub>Se<sub>2</sub> thin films, J. Appl. Phys. 94 (2003) 4341–4347. <https://doi.org/10.1063/1.1605813>.
- [30] S. Nishiwaki, S. Siebentritt, M. Giersig, M.C. Lux-Steiner, Growth model of CuGaSe<sub>2</sub> grains in a



Cu-rich/Cu-poor bilayer process, *J. Appl. Phys.* 94 (2003) 6864–6870.  
<https://doi.org/10.1063/1.1616642>.

- [31] D. Fuertes Marrón, A. Meeder, U. Bloeck, P. Schubert-Bischoff, N. Pfänder, R. Würz, S.M. Babu, T. Schedel-Niedrig, M.C. Lux-Steiner, Microstructural properties of CVD-grown CuGaSe<sub>2</sub> based thin film solar cells, *Thin Solid Films*. 431–432 (2003) 237–241. [https://doi.org/10.1016/S0040-6090\(03\)00264-5](https://doi.org/10.1016/S0040-6090(03)00264-5).
- [32] S. Ishizuka, CuGaSe<sub>2</sub> Thin Film Solar Cells : Challenges for Developing Highly Efficient Wide-Gap Chalcopyrite Photovoltaics, 1800873 (2019) 1–9. <https://doi.org/10.1002/pssa.201800873>.
- [33] A. Hultqvist, C. Platzer-Bjrkman, E. Coronel, M. Edoff, Experimental investigation of Cu(In<sub>1-x</sub>Ga<sub>x</sub>)Se<sub>2</sub>/Zn(O<sub>1-z</sub>S<sub>z</sub>) solar cell performance, *Sol. Energy Mater. Sol. Cells*. 95 (2011) 497–503. <https://doi.org/10.1016/j.solmat.2010.09.009>.

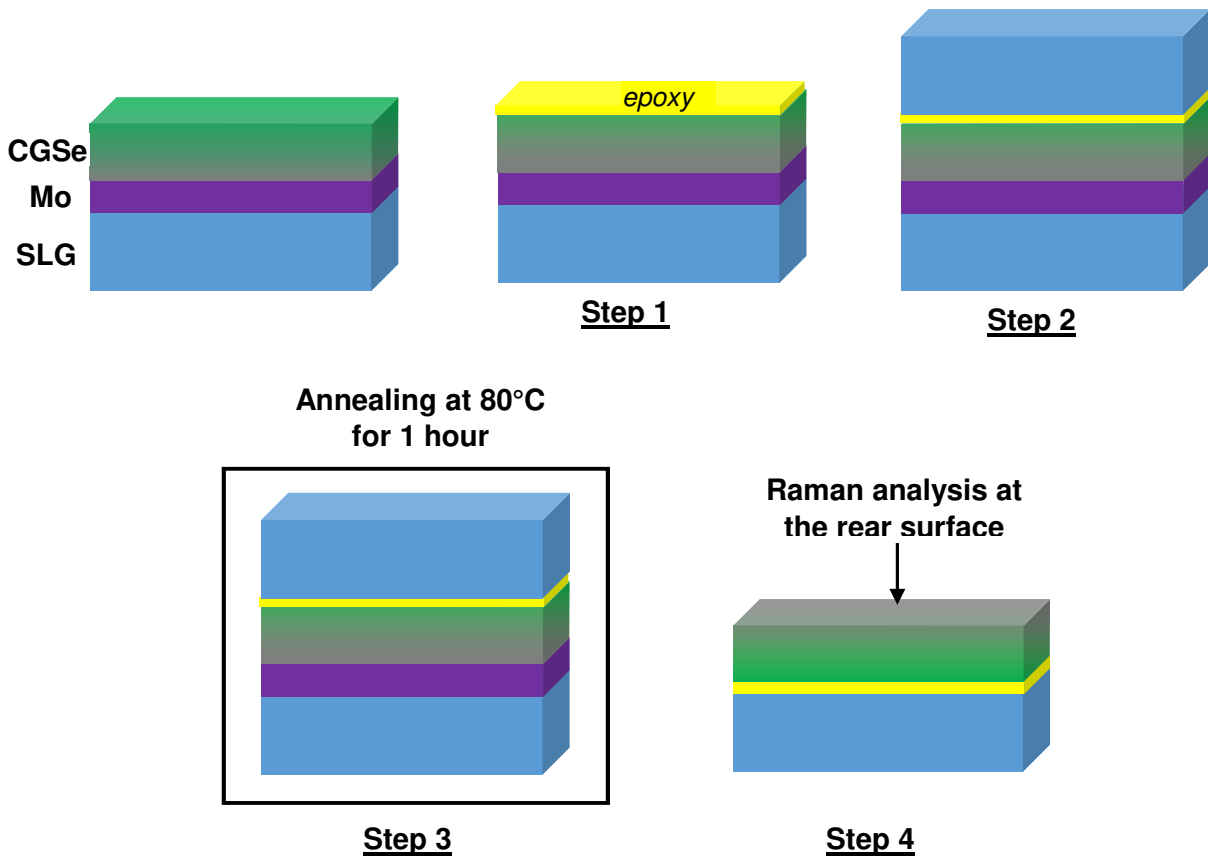


**Figure 1:** Schematic representation of the CGSe lift-off procedure and Raman analysis at the rear surface.

Step 1: after the end of CGSe deposition process, epoxy glue is applied onto the CGSe surface.

Step 2: the fresh epoxy glue is covered with soda-lime glass (SLG).

Step 3: the stack SLG/Mo/CGSe/epoxy/SLG is annealed at 80°C for 1 hour to polymerize the epoxy. Step 4: strain is applied to both SLG to separate the SLG/Mo from the CGSe/epoxy/SLG.

The rear CGSe surface is ready for Raman analyses

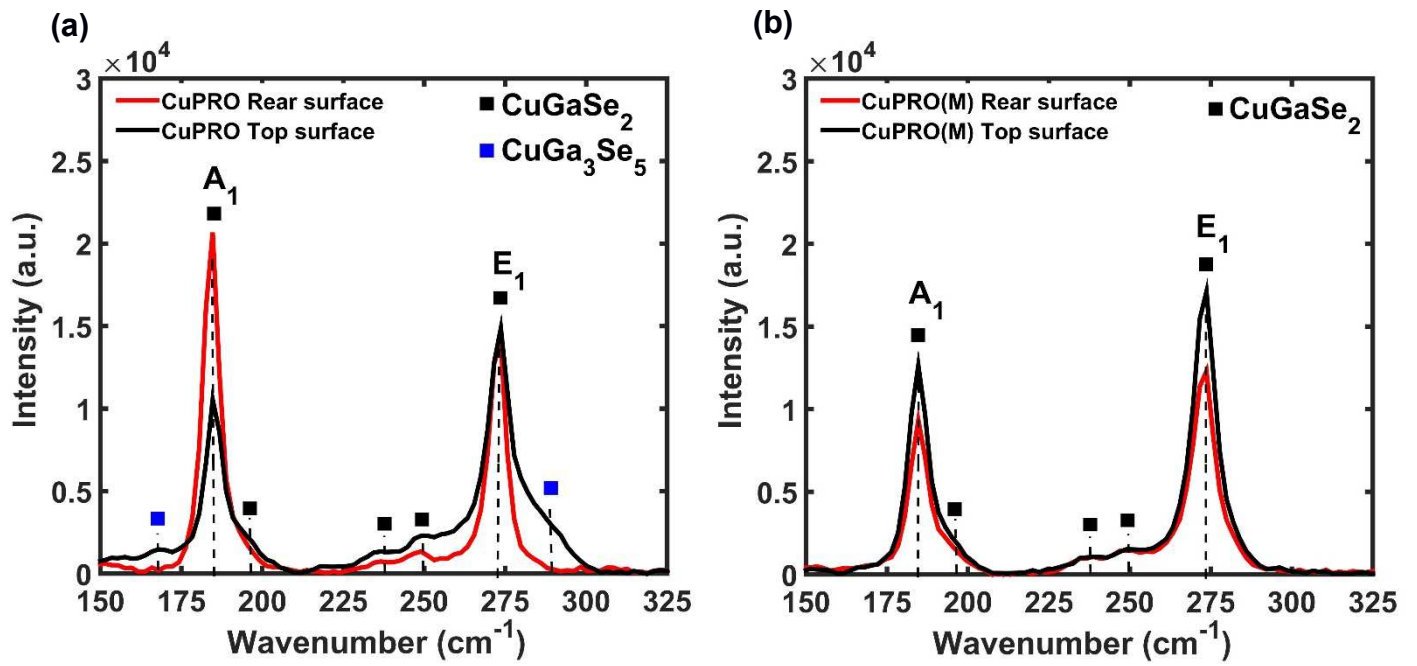


**Figure 2:** Micro-Raman spectrum at the top (black line) and the rear (red line), of a CGSe sample synthesized by a CuPRO (a) and a CuPRO(M) (b) process

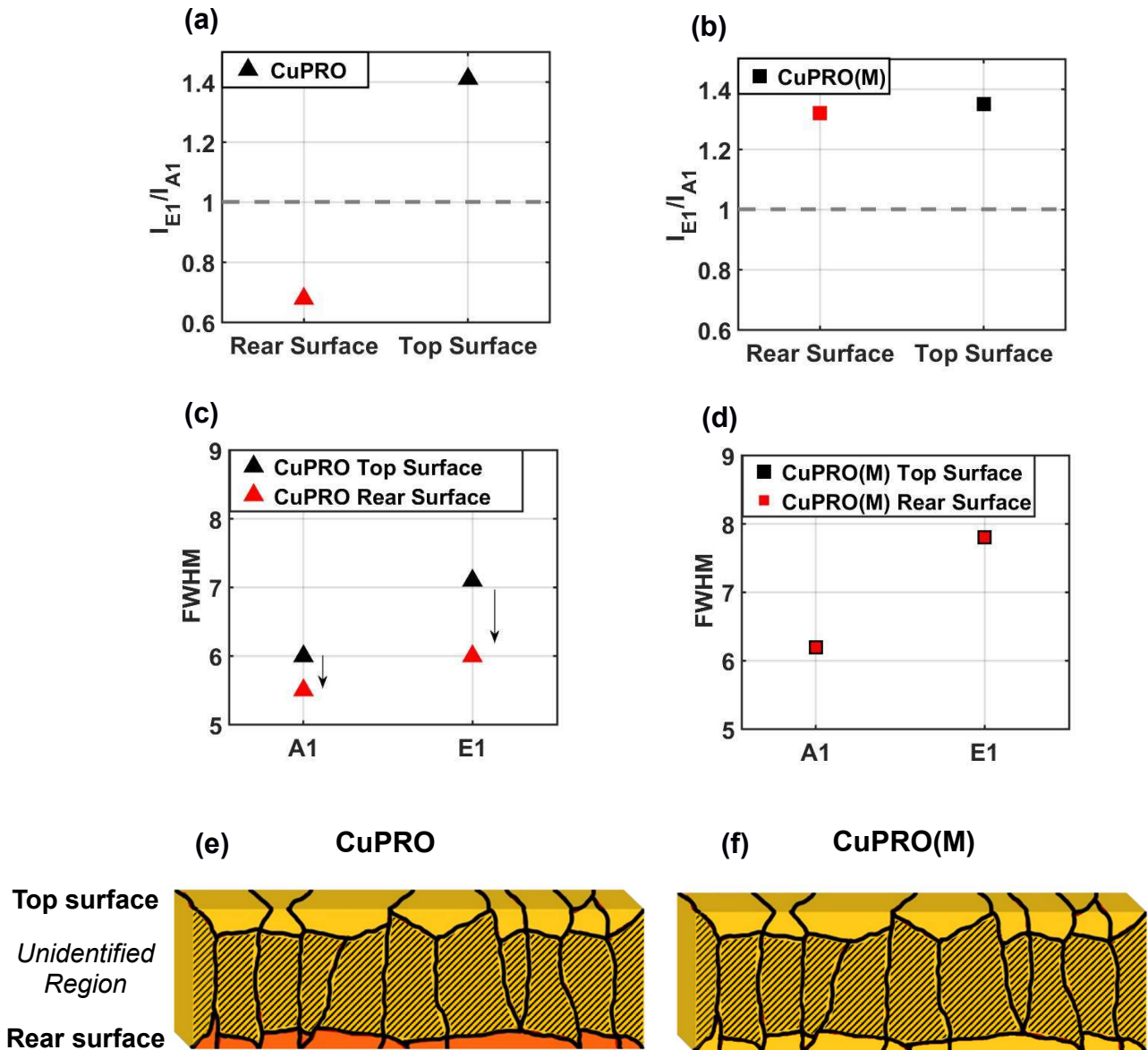


**Figure 3:**

**(a) and (b):** Graphical representation of intensity ratio of the A<sub>1</sub> and E<sub>1</sub> chalcopyrite vibrational modes ( $\Gamma = \frac{I_{E_1}}{I_{A_1}}$ ) at top and rear surfaces of CGSe grown by CuPRO and CuPRO(M).  $\Gamma$  values below 1 indicate important increase of the Cu content.

**(c) and (d):** Graphical representation of the FWHM of A<sub>1</sub> and E<sub>1</sub> chalcopyrite vibrational modes at the top and rear surfaces of CGSe grown by CuPRO and CuPRO(M). Low FWHM values indicate an increase of the Cu content.

**(e) and (f):** Schematic representation of CGSe films composition. Orange and yellow colors represent high and low Cu content, respectively. Stripped regions depict non-analyzed regions of the bulk.

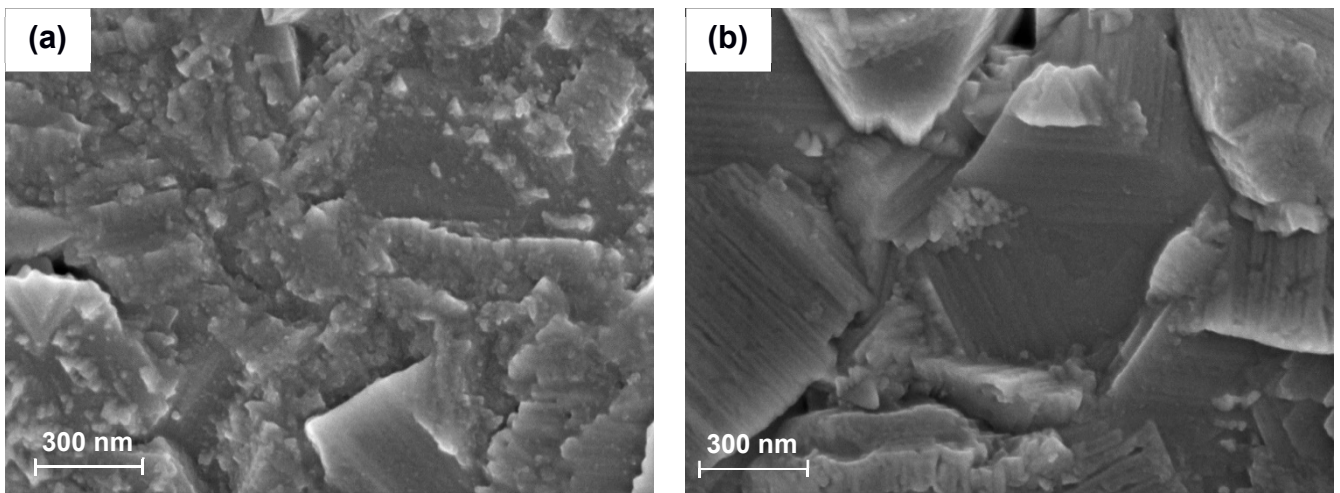


**Figure 4:** SEM surface images of the CGSe films deposited following CuPRO (a) and CuPRO(M) (b) co-evaporation processes.

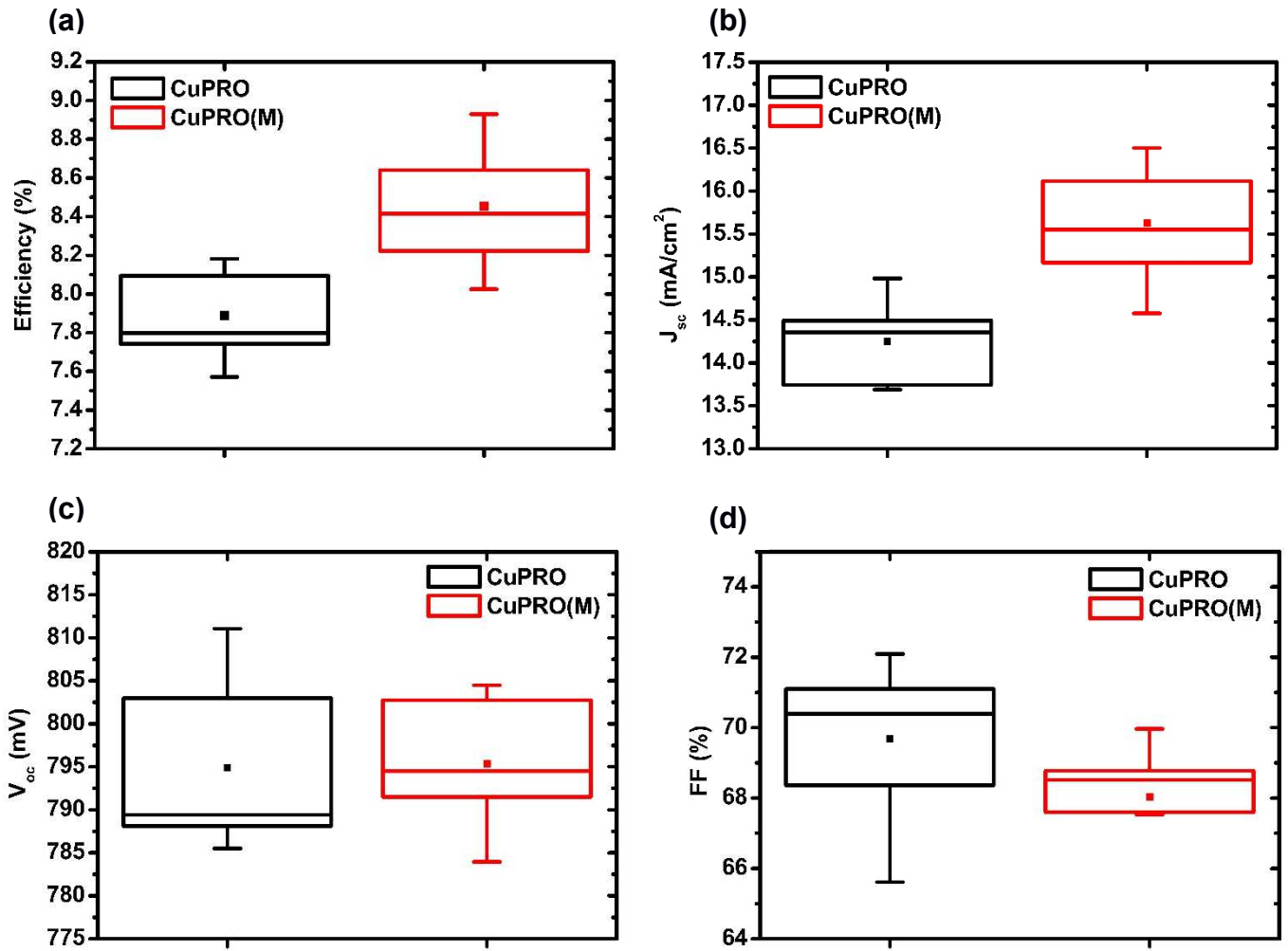


**Figure 5:** Statistical representation of investigated solar cell parameters; efficiency (a), short-circuit current density  $J_{sc}$  (b), open circuit voltage  $V_{oc}$  (c) and fill factor FF (d). Each boxplot gathers the parameters of 10 representative CGSe devices fabricated from absorbers grown by CuPRO (black) and CuPRO(M) (red).

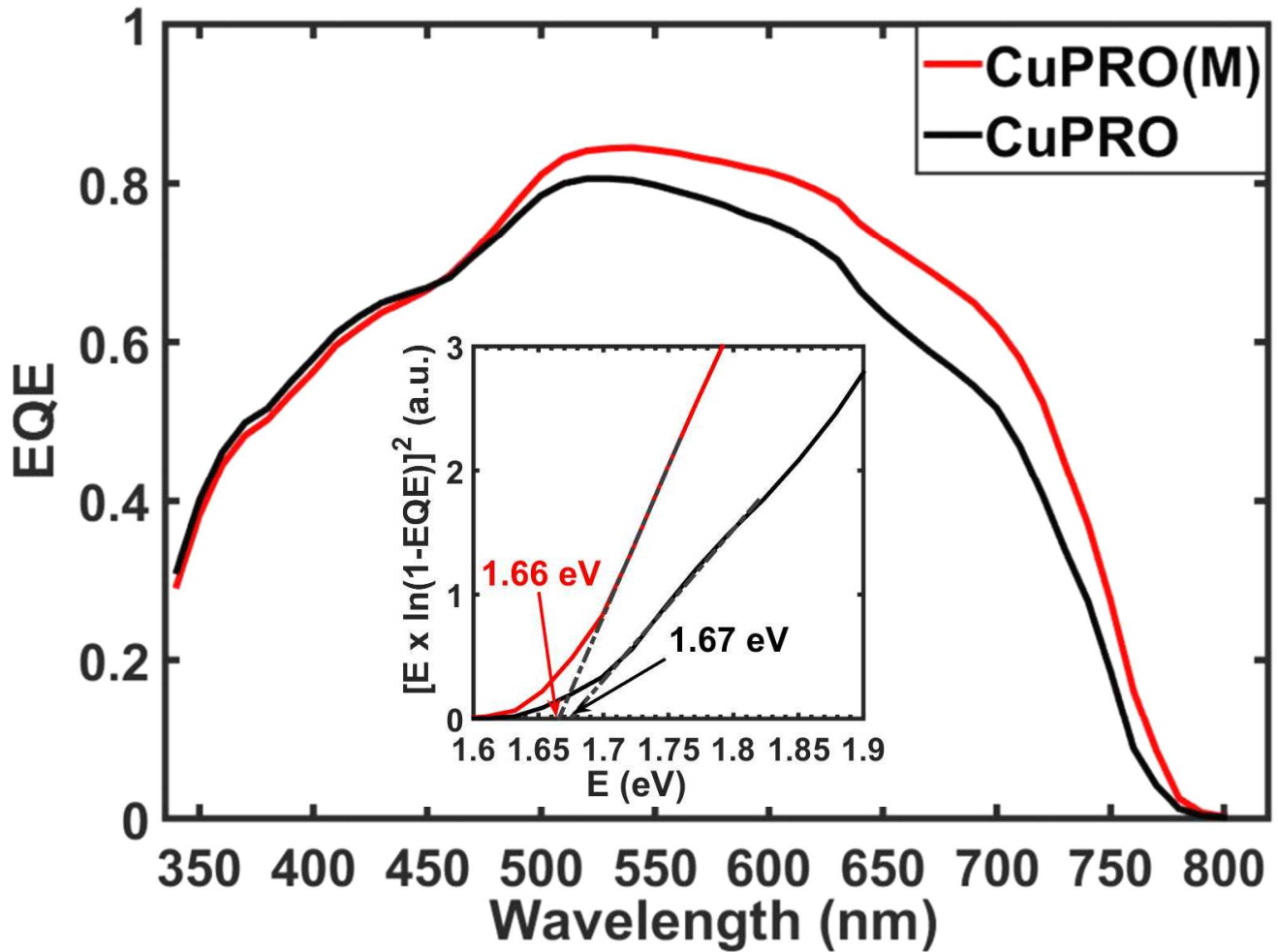


**Figure 6:** External quantum efficiencies (EQE) of solar cells demonstrating the highest efficiency achieved from CuPRO (black) and CuPRO(M) (red) absorbers. The inset curves show the estimated band gap energy from the  $[E \cdot \ln(1-EQE)]^2$  versus Energy plots.  $E_g = 1.665$  eV and  $1.670$  eV correspond to the band gap energy of the solar cell synthesized with the CuPRO(M) and CuPRO based absorber, respectively

**Table I:** Summary of the elemental concentration  $y=[\text{Cu}]/[\text{Ga}]$  measured by EDS using 20kV acceleration voltage and the co-evaporation process used to synthesize the CGSe thin films.

<b>Sample</b>	<b>y</b>	<b>Co-evaporation process</b>	<b>Relaxation stages</b>
#1963	$0.90 \pm 0.03$	CuPRO	none
#1969	$0.90 \pm 0.03$	CuPRO(M)	2



**Table II:** Photovoltaic parameters of best devices fabricated within the frame of this study (both are covered with MgF<sub>2</sub> Anti-Reflective Coating).

<b>Co-evaporation process</b>	<b><math>J_{sc}</math> (mA/cm<sup>2</sup>)</b>	<b><math>V_{oc}</math> (mV)</b>	<b><math>FF</math> %</b>	<b><math>\eta</math> %</b>
CuPRO	14.4	792	71.6	8.2
CuPRO(M)	16.1	792	70.0	8.9